MINISTRY OF EDUCATION AND TRAINING

VIETNAM ACADEMY OF SCIENCE AND TECHNOLOGY

GRADUATE UNIVERSITY OF SCIENCE AND TECHNOLOGY

CAO THI BICH

HYBRID ENTANGLEMENT, HYPERENTANGLEMENT AND THEIR APPLICATIONS FOR TELEPORTATION, CONTROLLED REMOTE STATE PREPARATION AND CONTROLLED REMOTE IMPLEMENTATION OF OPERATORS

SUMMARY OF PHYSICS DOCTORAL THESIS

Major: Mathematical and Theoretical Physics

Code: 9 44 01 03

HA NOI – 2023

The project was completed at: Graduate university of science and technology, Vietnam academy of science and technology

Supervisor 1: Assoc. Prof. Nguyen Ba An
Supervisor 2: Assoc. Prof. Nguyen Hong Quang

Reviewer 1: Assoc. Prof. Do Huu Nha
Reviewer 2: Assoc. Prof. Do Van Nam
Reviewer 3: Assoc. Prof. Nguyen Huy Viet

The thesis can be found at:
- Library of Academy of Science and Technology
- National Library of Vietnam

INTRODUCTION

Motivation

Quantum entanglement arguably exposes the most salient and counterintuitive feature of quantum theory, which, in Schrodinger's words, is "the characteristic trait of quantum mechanics, the one that enforces its entire departure from classical lines of thought". Nowadays, entanglement has widely been recognized as exhibiting nonlocal correlations in the magical quantum world that has no counterparts in our everyday-life classical world. It serves as an utmost vital resource in quantum information processing and quantum computing. State of a subsystem can be described in terms of any possible degree of freedom (DOF). In physical practice there are many DOFs. Take optical qubits (photons or light beams) for example. A photon can be described by polarization degree of freedom (P-DOF). A photon can also be described by spatial-path degree of freedom (S-DOF). As for a light beam qubit (also called 'logical qubit' or 'qumode'), it can be described by continuous variable degree of freedom (CV-DOF) in terms of a linear superposition of non-identical coherent states. If one and the same DOF is used to entangle two-dimensional subsystems, then such entanglement is regarded as usual. A new unusual kind (i.e., different from the above usual kind) of entanglement which bears the name 'hybrid entanglement' may be formed across different DOFs. Another new unusual kind of entanglement, called hyperentanglement, may exist as well at the same time in multiple (i.e., more than one) DOFs. Of interest is the optical domain, some task such as quantum cryptography, quantum dialogue and so on were investigated very intensively using quantum resources in terms of usual entanglement. However, the usual entanglement proves to be not good enough for various practical applications. That is why 'unusual' entanglements, namely, hybrid entanglement and hyperentanglement, come into the scene! But before exploiting such 'unusual' entanglements scientists should first be able to produce them in the labs and then propose desired protocols based on them.

As is well known, information can be encoded in either a DV state like (qubit) to be processed by the discrete-variable (DV) toolbox or a CV state like (qumode) to be processed by the CV toolbox. The former (latter) approach is called DV (CV) approach. Each approach has its advantages and drawbacks. Depending on the technology level a given remote node uses its own approach, either DV or CV

one, so the global network is a kind of heteronetwork. Since some operations prove to be better within the CV approach while others might be more efficient within the DV one, combining both approaches is a good idea in exploiting the advantages or/and avoiding drawbacks of each approach. For that combined approach to work interfacing between DV and CV encodings (in finite and infinite Hilbert spaces, respectively) should be possible. Such interconnections between remote quantum processors within the global heteronetwork can be implemented via hybrid entanglement. Usual and hybrid entanglements have been very useful to many practical tasks that cannot be executed without using such entangled resources. Then, why hyperentanglement is needed? Straightforwardly, hyperentanglement enables enhancing channel capacity: a bipartite usual or hybrid entangled state carries only 2 bits of information, but the information amount contained in a bipartite hyperentangled state within M different DOFs is bits, thus reducing quantum resource consumption and speeding up quantum algorithms. More meaningfully, hyperentanglement improves implementing many important protocols.

The problems as mentioned above, in our opinion, are new at the present time. The scientific significance and necessity are clear because their aims to connect quantum computers to achieve the high computing power needed for future computing needs. For these reasons, we carry out the project "Hybrid entanglement, Hyperentanglement and their applications for controlled quantum teleportation, controlled remote state preparation and Controlled remote implementation of operators".

Aims of the thesis

(i) Constructing new schemes to generate new/necessary types of optical hybrid entanglement and multipartite hybrid entangled states for quantum teleportation, remote state preparation protocols.
(ii) Using existing or newly-constructed types of optical hybrid entanglement to perform various protocols for controlled quantum teleportation between CV and DV states across lossy environment.
(iii) Constructing new schemes to generate new/necessary types of optical hyperentanglement.
(iv) Proposal of protocols for controlled remote state preparation and controlled

remote implementation of operators.

Structure of the thesis

Besides the Introduction, the Conclusion, the thesis consists of three main chapters arranged as follows:

- Chapter 1: Some of basic concepts
- Chapter 2: Hybrid entanglement and its applications for controlled quantum teleportation.
- Chapter 3: Hyperentanglement and its applications for controlled bidirectional remote hyperstate preparation and controlled remote implementation of operators.

CHAPTER 1. SOME OF BASIC CONCEPTS

1.1 Linear optical devices

1.1.1. Beam splitter

Beam splitters (BS) are widely used in optical quantum information processing, especially in generation of coherent states and their possible superpositions. Realistically, a beam splitter is simply realized by a partly silvered mirror so that it works as partly transmitting and partly reflecting an incident light beam that comes to it. When the input states are $|n\rangle_a|m\rangle_b$, the output state will be an entangled state, while the input states are $|\alpha\rangle_a|\beta\rangle_b$, the output is the product state.

1.1.2. Phase shifter

Another necessary optical device is phase shifter (PS), which could simply be a length of optical fiber. The phase shifter's effect is altering the phase of an incident light beam.

1.1.3. Displacement operator

Displacement operator $\hat{D}(\alpha)$ is a very useful operator for computations with coherent states. It is represented as

$$\hat{D}(\alpha) = e^{\alpha a^{+} - \alpha^{*} a}. \tag{1}$$

It is then clear that a coherent state is a result when applying the displacement operator on the vacuum state

$$\hat{D}(\alpha)|0\rangle = |\alpha\rangle. \tag{2}$$

1.1.4. The others linear optical devices

Several essential optical devices to mention are: Polarization beam splitter (PBS), Half wave plate (HWP) and Quarter wave plate (QWP)

PBS is a beam splitter that let the photons in the horizontally polarized state $|H\rangle$ through, while let the photon in the vertically polarized state $|V\rangle$ reflect.

HWP is a device used to rotate the polarization state. Namely, it converts H state to V state and vice versa.

QWP is a device used to convert linearly polarized light into circularly polarized light. Specifically, QWP acts as a Hadamard operator.

1.2. Interaction between photons via cross-Kerr effect

The interaction between photons is very important since they are the key element to implement multi-qubit logic gates, which complete building blocks for quantum computation and quantum information. However, photons do not interact with each other in the vacuum, thus motivating to find a way to acquire photon-photon interactions or nonlinearities sufficient for optical quantum information processing. For this purpose, cross-Kerr effect, which is essentially a phenomenon that nonlinear medium facilitates photon-photon interactions, has been considered as a remarkable method.

1.3. Homodyne detection

In the application of non-classical light, the homodyne detection provides the measurement of the quadrature operators of the electromagnetic field. Balanced

homodyne detection allows to perform Bell measurements of continuous variable states with deterministic manner hence it is applied in quantum teleportation of continuous variable quantum states. Balanced homodyne detection is also studied to fully determine the properties of quantum states such as phase squeezed state, amplitude squeezed state or the superposition of macroscopic states through tomography technology. In these citations, the authors used quantum tomography technology to measure the Wigner distribution and determine the density matrix of states. From that, it is possible to determine the full information of that state. In addition, the balanced homodyne detection is also applied in the protocol for establishing the quantum correlation of the EPR state and it is also used to demonstrate the non-classical properties of the electromagnetic field in electrodynamics.

1.4. Adaptive phase measurements in linear optical quantum computation

Adaptive phase measurement based on the extension of the homodyne measurement and thus the measurement results have a continuous spectrum, which is not same the discrete values produced by a photon counter. Consider a single-mode pulse and a reference field as a coherent state of large amplitude. This reference field has the same frequency as the pulse. Here, the phase of the reference field is $\phi(t)$, which is fixed as a constant for the homodyne measurement and as a linear function of time for the heterodyne measurement. "Adaptive" in adaptive phase measurement means that the performance of the next stage will depend on the results of the previous stage. The pulse is combined with the reference field through a balanced beamsplitter. The principle of this measurement is that the oscillation phase of the reference field is continuously adjusted during the measurement and depends on the result of the difference in the photon current between the two modes. This adaptive dyne detection is useful for estimating the unknown phase of an optical pulse. Superposition state preparation and quantum gate design are two typical examples of the applications of adaptive phase measurement.

1.5. Photodetector

Photodetector also known as photosensor, is a sensor that converts photons of light or electromagnetic radiation into an electrical signal. The photodetector is one of the important components in optoelectronic integrated circuits. It is widely used in optical communication, optical interconnection and biomedical imaging systems, and it generally operates from visible to near-infrared wavelengths. Photodetector is used mostly in the tasks of this thesis.

CHAPTER 2. HYBRID ENTANGLEMENT AND ITS APPLICATIONS FOR CONTROLLED TELEPORTATION

In this chapter, in Section 2.1, we design a new scheme to generate with unit fidelity a type of hybrid entanglement between a macroscopic polarized coherent state and a single polarized photon. In Section 2.2, we propose the DV-CV hybrid entangled state generation protocol between four modes. In Section 2.3, we present the hybrid controlled teleportation protocols taking into account the dissipation effect caused by the presence of losses in the environment surrounding the participants.

2.1. Scheme to generate the DV-CV hybrid entanglement between a polarized coherent state and a polarized single photon

We propose a new displacement-free scheme to create hybrid entanglement of the form

$$|\Psi\rangle_{AB} = \frac{1}{\sqrt{2}} \left(|\alpha_H\rangle_A |H\rangle_B + |-\alpha_V\rangle_A |V\rangle_B \right). \tag{3}$$

Necessary input states are

$$|\Gamma\rangle_1 = N(\beta) \left(|\beta_H\rangle + |-\beta_H\rangle \right)_1, \tag{4}$$

$$|\Lambda\rangle_{1'} = |\beta_H\rangle_{1'}, \tag{5}$$

$$|\Theta\rangle_{34} = \frac{1}{\sqrt{2}} \left(|H\rangle_3 |V\rangle_4 + |V\rangle_3 |H\rangle_4 \right), \tag{6}$$

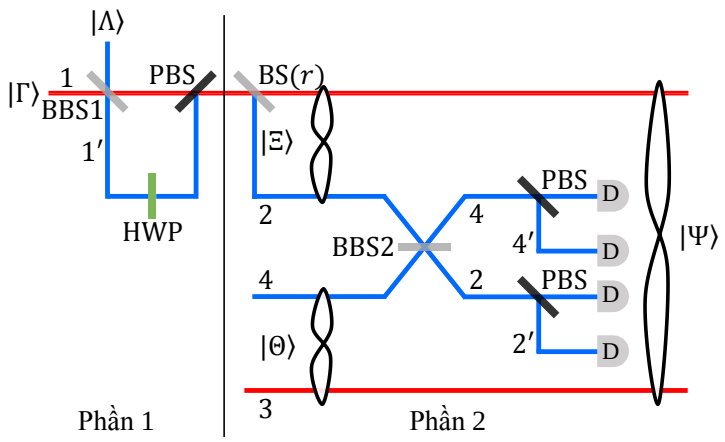

Figure 1: Scheme to generate the DV-CV hybrid entanglement between a polarized coherent state and a polarized single photon.

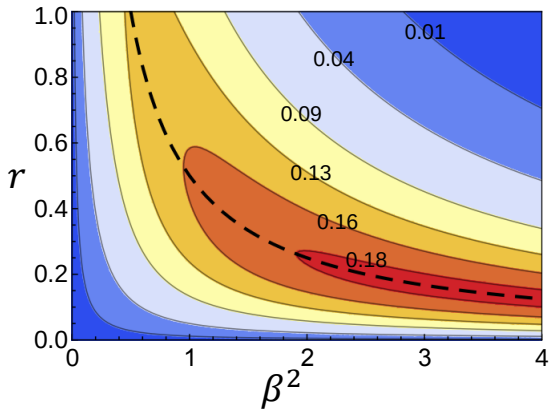

Figure 2: Total success probability of the scheme $P_T = 4P$ with P given in 7 as a function of β^2 and r. The (black) dashed line represents the optimal reflectivity, $r^{\text{peak}} = 1/(2\beta^2)$, optimizing the total success probability P_T for $\beta^2 > 1/2$. Selected contour values for P_T are marked.

where β is assumed to be real for simplicity and $N(\beta) = [2(1 + e^{-2\beta^2})]^{-1/2}$ is a normalization constant. Our scheme to entangle a polarized coherent state and a polarized single photon into the hybrid entanglement of the form (3) is visually illustrated in Figure 1. Total success probability of the scheme $P_T = 4P$ with P given in

$$P = \langle \Sigma' | \, \Pi_{1(2,3,4)} | \Sigma' \rangle = \frac{N^2(\beta) f_1^2(\gamma)}{4} = \frac{r\beta^2 e^{-2r\beta^2}}{4(1 + e^{-2\beta^2})}. \tag{7}$$

It is plotted in Figure 2 as a function of β^2 and r. For $\beta^2 \leq 0.5$, the probability P_T increases monotonically with increasing r. For $\beta^2 > 0.5$, as $r\beta^2 \exp(-2r\beta^2)$ peaks at $2r\beta^2 = 1$, the probability P_T peaks at $r = r^{\text{peak}} = 1/(2\beta^2)$ which is displayed as a (black) dashed line in Figure 2.

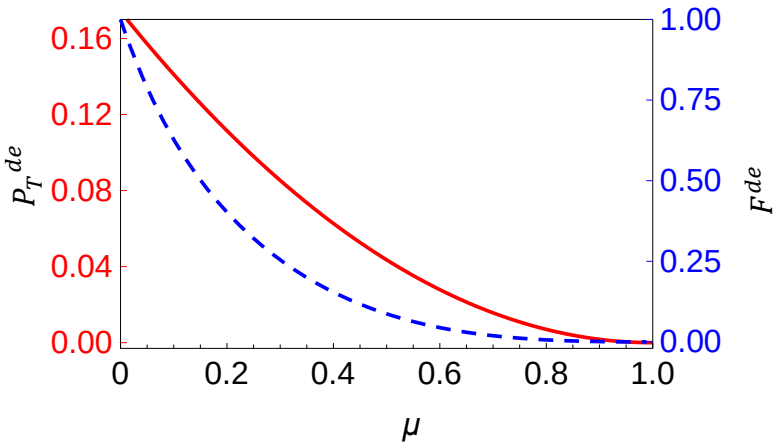

Figure 3: Total success probability $P_T^{\rm de}$ (solid line) and fidelity $F^{\rm de}$ (dashed line), respectively, as functions of the decoherence strength.

2.1.1. Effect of Decoherence

The decoherence process we are interested in is photon loss, which is modeled by the master equation

$$\frac{d\rho}{d\tau} = \hat{\mathcal{D}}\rho. \tag{8}$$

The input density operator ρ then depends on the interaction time τ and the decay rate κ. Formally the time-dependent input density operator $\rho(\tau)$ can be written in the form $\rho(\tau) = e^{\hat{\mathcal{D}}\tau}\rho(0)$

$$\rho(\tau) = \rho_1(\tau) \otimes \rho_{1'}(\tau) \otimes \rho_{34}(\tau). \tag{9}$$

Recomputing calculations with the decohered inputs yields the total success probability and the fidelity under the effect of decoherence as follows

$$P_T^{\rm de} = \nu^2 P_T, \tag{10}$$

$$F^{\rm de} = \frac{1}{2}\nu^2 |\langle\alpha|\alpha\nu\rangle|^2 (1 + C_1). \tag{11}$$

The total of the success probability and the fidelity which depend on the decoherence strength are plotted in Figure 3.

2.1.2. Realistic input resources

Precise generation of these cat states in general is a daunting task; in most optical experiments, they are replaced with squeezed resources. Specifically, for small

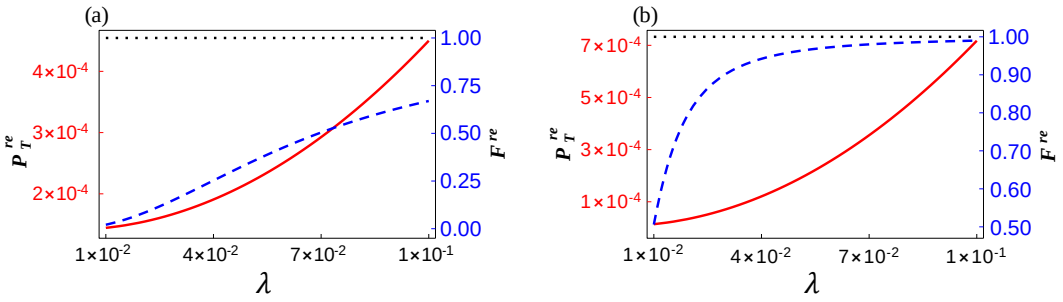

Figure 4: Total success probability $P_T^{\rm re}$ (solid line) and fidelity $F^{\rm re}$ (dashed line) in dependence on the type-II SPDC strength λ when using (a) the squeezed vacuum with $s = -0.43358$ as an approximation to an even cat state of amplitude 0.7 and (b) the squeezed single photon with $s = 0.16056$ as an approximation to an odd cat state of amplitude 0.7. In both panels, the dot-dashed line represents the unit fidelity (i.e., when the input states are perfect) and the reflectivity r is chosen to be 0.1.

amplitudes even and odd cat states can be very well approximated respectively by a squeezed vacuum and a squeezed single photon. While the former state can be generated deterministically via vacuum squeezing, production of the latter typically involves subtracting one photon which is of probabilistic nature and of low efficiency. In that sense, approximate even cat states would be more experimentally accessible than approximate odd ones. In Fock-state basis, the squeezed vacuum and the squeezed single photon are respectively of the forms

$$|\mathrm{sv}\rangle = \sum_{n=0}^{\infty} \frac{(-\tanh s)^n}{(\cosh s)^{1/2}} \frac{\sqrt{(2n)!}}{2^n n!} |2n\rangle, \tag{12}$$

$$|\mathrm{ss}\rangle = \sum_{n=0}^{\infty} \frac{(\tanh s)^n}{(\cosh s)^{3/2}} \frac{\sqrt{(2n+1)!}}{2^n n!} |2n+1\rangle, \tag{13}$$

where in both equations s is the squeezing parameter and assumed to be real.

Besides the cat states, the entangled polarization photon pair is also a requisite input state in our scheme. In practice, the state $|\Theta\rangle_{34}$ is routinely generated via the type-II spontaneous parametric down conversion (SPDC) process, in which a pump photon is split into two daughter ones (signal and idler) entangled in orthogonal polarizations. The output of such process unavoidably includes a large vacuum component and is approximately given by

$$|\mathrm{SPDC}\rangle_{34} \simeq \sqrt{1-\lambda^2}|0\rangle_3|0\rangle_4 + \lambda|\Theta\rangle_{34} + \mathrm{O}(\lambda^2), \tag{14}$$

where λ is the (dimensionless) SPDC interaction strength typically of order 10^{-2}. In particular, the total realistic success probability $P_T^{\rm re}$ and the realistic fidelity

$F^{\rm re}$ taking into account the realistic input resources are found as

$$P_T^{\rm re} = (1-\lambda^2)P_{T,0}^{\rm re} + \lambda^2 P_{T,\Theta}^{\rm re}, \tag{15}$$

$$F^{\rm re} = \frac{(1-\lambda^2)P_{T,0}^{\rm re}F_0^{\rm re} + \lambda^2 P_{T,\Theta}^{\rm re}F_\Theta^{\rm re}}{P_T^{\rm re}} = \frac{\lambda^2 P_{T,\Theta}^{\rm re}}{P_T^{\rm re}}F_\Theta^{\rm re}. \tag{16}$$

In Figure 4 we plot total success probability $P_T^{\rm re}$ (solid line) and fidelity $F^{\rm re}$ (dashed line) in dependence on the type-II SPDC strength λ when using (a) the squeezed vacuum with $s = -0.43358$ as an approximation to an even cat state of amplitude 0.7 and (b) the squeezed single photon with $s = 0.16056$ as an approximation to an odd cat state of amplitude 0.7. In both panels, the dot-dashed line represents the unit fidelity (i.e., when the input states are perfect) and the reflectivity r is chosen to be 0.1.

2.1.3. Imperfections in balanced beam splitters

We assume that the PBSs and the HWP are perfect but consider the circumstance when the two BBSs could be slightly unbalanced. To this end, we introduce imperfection parameters ϵ_k for $k = 1, 2$ defined via the reflectivity and the transmissivity of each imperfect BBS as

$$r_k = 1/2 - \epsilon_k, \;\; t_k = 1/2 + \epsilon_k. \tag{17}$$

Intuitively, we wish ϵ_k to be very small compared to 1/2 to obtain good total success probability and fidelity.

Detailed expressions for $P_j^{\rm im}$ and $F_j^{\rm im}$, we highlight essential results only. Generally, $P_j^{\rm im}$ and $F_j^{\rm im}$ are dependent on ϵ_1 and ϵ_2. For example, regarding the measurement Π_1 we find

$$P_1^{\rm im} = N^2(\beta)\left[(r_2^2+t_2^2)r\beta^2 e^{-2r\beta^2} + (r_2^2-t_2^2)\gamma_1\gamma_2 e^{-2\beta^2}\right] \tag{18}$$

and

$$F_1^{\rm im} = \frac{N^2(\beta)e^{-2r\beta^2}}{4P_1^{\rm im}}\left[\gamma_2 f_0(\delta_1)(r_2\langle\delta|\delta_2\rangle - t_2\langle-\delta|\delta_2\rangle) + \gamma_1 f_0(\delta_2)\langle\delta|\delta_1\rangle\right]^2. \tag{19}$$

However, we find that the total success probability is remarkably the same as in the ideal case, that is,

$$\sum_{j=1}^{4} P_j^{\rm im} = P_T, \tag{20}$$

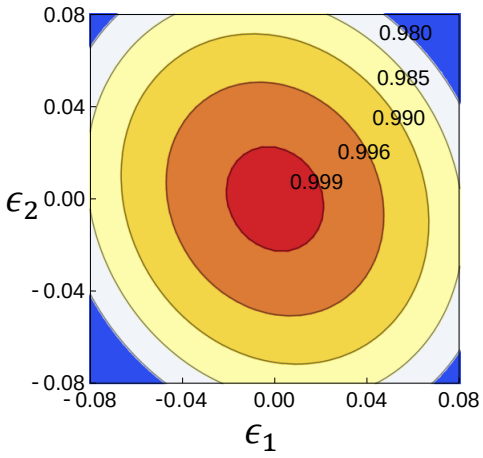

Figure 5: Average fidelity $\bar{F}^{\rm im}$ in variation with respect to the BBS imperfection parameters ϵ_1 and ϵ_2.

where $P_T = 4P$ with P given in Eq. (7). This shows that the scheme total success probability is completely insensitive to BBS imperfections. For analysis of the fidelity, we define its average

$$\bar{F}^{\rm im} = \frac{\sum_{j=1}^{4} P_j^{\rm im} F_j^{\rm im}}{\sum_{j=1}^{4} P_j^{\rm im}}, \tag{21}$$

which depends on both ϵ_1 and ϵ_2. In Figure 5, we plot $\bar{F}^{\rm im}$ as a function of ϵ_1 and ϵ_2. As seen clearly, $\bar{F}^{\rm im}$ remains very high (≥ 0.980) for ϵ_1 and ϵ_2 ranging from -0.08 to 0.08. The value of $\bar{F}^{\rm im}$ approaches unit when ϵ_1 and ϵ_2 are close to zero. Concretely, $\bar{F}^{\rm im} \geq 0.999$ for $|\epsilon_1|, |\epsilon_2| \leq 0.02$.

2.1.4. Inefficient detectors

A crucial requirement in our scheme is that photodetectors are able to resolve photon numbers with high fidelity. However, these detectors in practice always operate with some finite imperfection. We thus take into account realistic inefficient detectors whose figure of merit is characterized by the efficiency η with $\eta \in [0, 1]$. Mathematically, an imperfect detection of an n-photon state with efficiency η is modeled by a positive operator-valued measurement (POVM)

$$E_{\eta,a}^{(n)} = \sum_{k=0}^{\infty} C_{n+k}^{k} \eta^n (1-\eta)^k |n+k\rangle_a \langle n+k|, \tag{22}$$

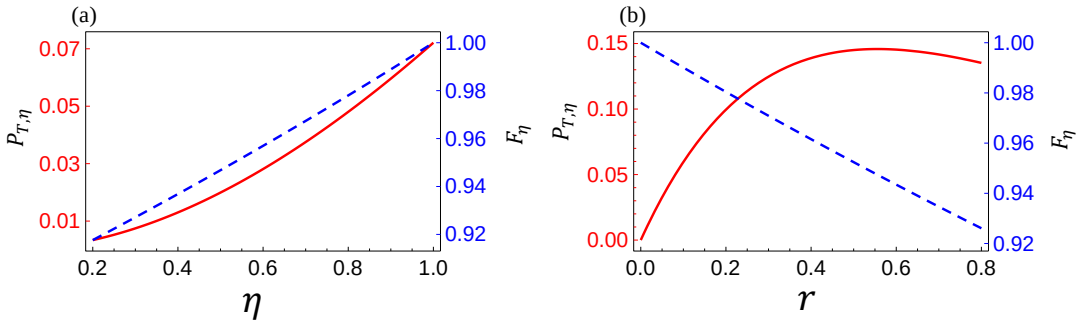

Figure 6: Total probability $P_{T,\eta}$ (solid line) and fidelity F_η (dashed line) in dependence on (a) the detector efficiency η and (b) the reflectivity r. In panel (a) the reflectivity r is 0.1, while in panel (b) the photodetector efficiency η is 0.9. In both panels, we assume perfect input states of which the input even cat state has an amplitude $\beta = 1$.

where a denotes the detected photon mode. The perfect measurement Π_1 is then rewritten as

$$\Pi_{1,\eta} = E^{(0)}_{\eta,2} \otimes E^{(1)}_{\eta,2'} \otimes E^{(1)}_{\eta,4} \otimes E^{(0)}_{\eta,4'}, \tag{23}$$

and similarly for Π_2, Π_3 and Π_4.

In the presence of inefficient detectors and assuming the input states given in Eqs. (4) - (6) are perfect, the total success probability and the fidelity are given by

$$P_{T,\eta} = \frac{r\beta^2\eta^2 e^{-2r\beta^2\eta}}{1+e^{-2\beta^2}}, \tag{24}$$

$$F_\eta = \frac{1+e^{-2r\beta^2(1-\eta)}}{2}. \tag{25}$$

In Figure 6 we plot $P_{T,\eta}$ (solid line) and F_η (dashed line) with respect to (a) the detector efficiency η and (b) the reflectivity r.

2.2. Generation of a four-mode hybrid entanglement between the coherent state and the single-rail qubit state

The hybrid DV-CV four-party quantum entanglement has form

$$|\Gamma(\alpha)\rangle_{1234} = \frac{1}{\sqrt{2}}(|\alpha,\alpha,0,0\rangle + |-\alpha,-\alpha,1,1\rangle)_{1234}. \tag{26}$$

In order to prepare the pure hybrid entangled state, we need the following initial state

$$|\Psi_0(\alpha)\rangle_{klmn} = \left|\Phi(\alpha\sqrt{2})\right\rangle_{kl} |\Phi(2\alpha)\rangle_{mn}, \tag{27}$$

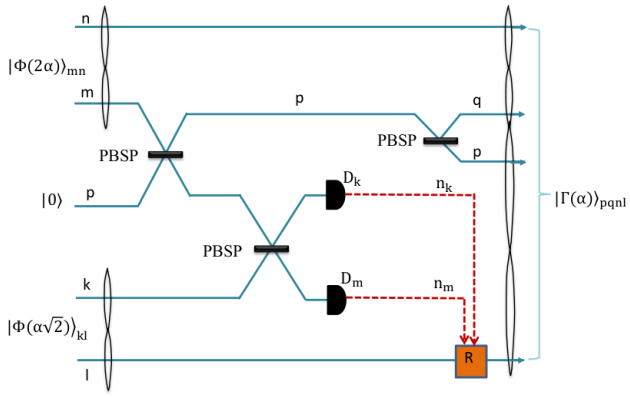

Figure 7: Quantum circuit to produce the hybrid entanglement defined by Eq. (32). BS denotes a beam-splitter, which acts on two modes as $BS_{xy}(\pi/4) = exp[\pi(a_x^+ a_y - a_y^+ a_x)/4]$. The solid line labeled n (k, l, m, n, p and q) represents mode n (k, l, m, n, p and q). D_k and D_m are photo-detectors to count the photon numbers in the corresponding modes. The dashed lines represent the numbers n_k and n_m of detected photons. $R = I$, X, Z or XZ conditioned on the detected numbers of photons.

where

$$|\Phi(\gamma)\rangle_{xy} = \frac{1}{\sqrt{2}}(|\gamma, 0\rangle + |-\gamma, 1\rangle)_{xy}. \tag{28}$$

Our three-step scheme for preparation of the state (32) is sketched in Figure 7. The total probability P_Γ for successful preparation of the quantum channel $|\Gamma\rangle$ in Eq. (32) is

$$P_\Gamma = \frac{3}{2}(P_{even\neq 0,0} + P_{odd,0}) = \frac{3}{4}(1 - e^{-4|\alpha|^2}), \tag{29}$$

which saturates to 75% for $|\alpha| \geq 1.3$. However, the probabilistic feature of the hybrid entanglement preparation scheme is not an issue because the state preparation process is regarded as an off-line procedure.

2.3. Teleporting DV qubit to CV qubit and vice versa via DV-CV hybrid entanglement across lossy environment supervised simultaneously by both DV and CV controllers

We shall consider these tasks separately. The first task is that Alice holds a single-rail qubit in state

$$|\psi_{DV}\rangle = a\,|0\rangle + b\,|1\rangle\,, \tag{30}$$

where $|0\rangle$ ($|1\rangle$) is the vacuum (the single-photon) state and a, b are unknown complex coefficients satisfying the normalization constraint $|a|^2 + |b|^2 = 1$. She needs to securely transfer to Bob the coefficients a, b in terms of a coherent-state qubit state

$$|\psi_{CV}(\alpha)\rangle = N(a\,|\alpha\rangle + b\,|-\alpha\rangle), \tag{31}$$

where $|\pm\alpha\rangle$ are coherent states with complex amplitudes $\pm\alpha$ and $N = N(a, b, \alpha) = (1 + 2Re(a^*b)e^{-2|\alpha|^2})^{-1/2}$ is to normalize the state $|\psi_{CV}(\alpha)\rangle$. The second task, inverse to the first one, is that Bob holds an unknown coherent-state qubit in state (31) and needs to securely transfer to Alice the coefficients a, b in terms of a single-rail qubit state (30). We aim at designing protocols such that both the two tasks are simultaneously supervised by two controllers Charlie and David, with Charlie being able to work only with DV single-rail states while David being only capable of manipulating CV coherent-state qubits. Each of the two above-formulated tasks could only be completed upon permission of both the controllers. To execute either of the two tasks by means of local operations and classical communication, the four parties Alice, Bob, Charlie and David should share in advance a relevant hybrid DV-CV four-party quantum entanglement in terms of the pure entangled state of the form

$$|\Gamma(\alpha)\rangle_{1234} = \frac{1}{\sqrt{2}}(|\alpha, \alpha, 0, 0\rangle + |-\alpha, -\alpha, 1, 1\rangle)_{1234}, \tag{32}$$

The modes of such quantum channel must be distributed so that Alice receives mode 4, David mode 2, Charlie mode 3 and Bob mode 1. During the modes' distribution photon losses occur due to interaction with the surrounding lossy environment or, in other words, the quantum channel suffers from dissipation. The dissipation effect can be described, within the framework of the Born-Markov

approximation at zero temperature, by the master equation

$$\begin{aligned}\rho_{1234}(\tau) &= \frac{1}{2}\{[|\tau\alpha\rangle_1\langle\tau\alpha| \otimes |\tau\alpha\rangle_2\langle\tau\alpha| \\ &\otimes|0\rangle_3\langle 0| \otimes |0\rangle_4\langle 0| \\ &+C\tau^2|\tau\alpha\rangle_1\langle-\tau\alpha| \otimes |\tau\alpha\rangle_2\langle-\tau\alpha| \\ &\otimes|0\rangle_3\langle 1| \otimes |0\rangle_4\langle 1| \\ &+C\tau^2|-\tau\alpha\rangle_1\langle\tau\alpha| \otimes |-\tau\alpha\rangle_2\langle\tau\alpha| \\ &\otimes|1\rangle_3\langle 0| \otimes |1\rangle_4\langle 0| \\ &+|-\tau\alpha\rangle_1\langle-\tau\alpha| \otimes |-\tau\alpha\rangle_2\langle-\tau\alpha| \\ &\otimes(\tau^2\,|1\rangle_3\,\langle 1| + (1-\tau^2)\,|0\rangle_3\,\langle 0|) \\ &\otimes(\tau^2\,|1\rangle_4\,\langle 1| + (1-\tau^2)\,|0\rangle_4\,\langle 0|)\}, \end{aligned} \tag{33}$$

where $C = e^{-4(1-\tau^2)\alpha^2}$ và $\tau = e^{-\gamma t/2}$.

In the first task. Suppose that Alice has a single-rail qubit A in an unknown state $|\psi_{DV}\rangle_A = (a\,|0\rangle + b\,|1\rangle)_A$ and she needs to teleport $|\psi_{DV}\rangle_A$ to Bob through a lossy environment so that Bob receives a coherent-state qubit of the form

$$|\psi_{CV}(\tau\alpha)\rangle_1 = N(a\,|\tau\alpha\rangle + b\,|-\tau\alpha\rangle)_1. \tag{34}$$

In order to perform the hybrid controlled teleportation in the Alice-to-Bob direction, each of the four parties should act properly as shown in Figure 8a.

Total probability of success $P_{DV\to CV}$ is given by

$$\begin{aligned}P_{DV\to CV} &= P_X + P_{XZ} \\ &= \frac{1}{16}[3(|b|^2(2-\tau^2) + |a|^2\tau^2) \\ &+ C\tau^2(a^*b + b^*a)e^{-2\tau^2\alpha^2}]. \end{aligned} \tag{35}$$

The fidelity $F_{DV\to CV}$ is determined by

$$\begin{aligned}F_{DV\to CV} &= {}_1\langle\psi_{CV}(\tau\alpha)|\rho_1^{(T)}(\tau)|\psi_{CV}(\tau\alpha)\rangle_1 \\ &= N^2(a,b,\tau\alpha)L^{\text{odd}}(\tau)\{|b(b+ae^{-2\tau^2\alpha^2})|^2 \\ &+ ((1-\tau^2)|b|^2 + \tau^2|a|^2)|(be^{-2\tau^2\alpha^2} + a)|^2 \\ &+ 2C\tau^2 Re[ab^*(ae^{-2\tau^2\alpha^2} + b)(a^* + b^*e^{-2\tau^2\alpha^2})]\}. \end{aligned} \tag{36}$$

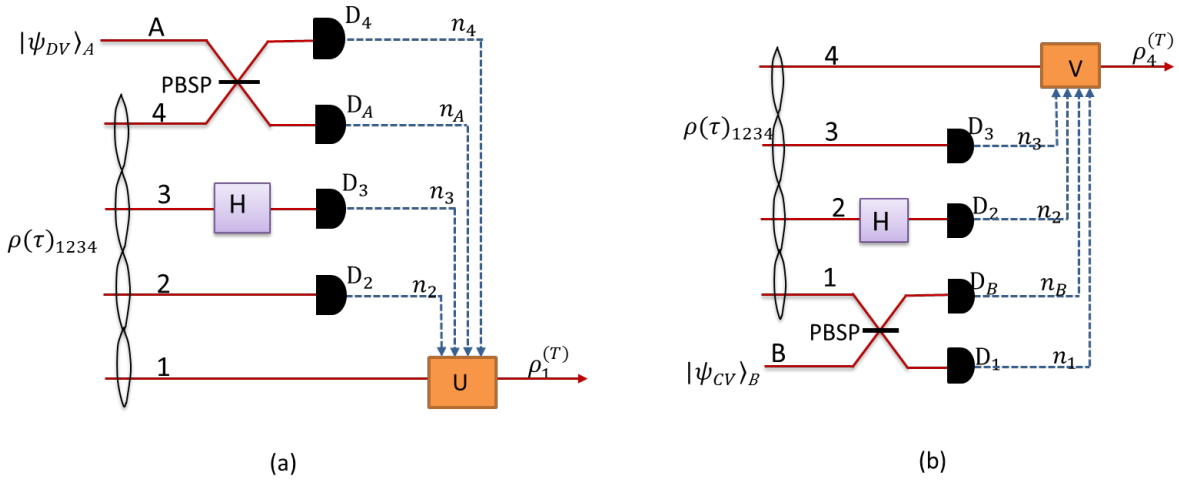

Figure 8: (a) Scheme for controlled teleportation from a DV state to a CV state. (b) Scheme for controlled teleportation from CV to DV state

In the second task, now Bob plays the role of a teleporter holding a coherent-state qubit in the CV state $|\psi_{CV}(\tau\alpha)\rangle_B = N(a\,|\tau\alpha\rangle + b\,|-\tau\alpha\rangle)_B$ with parameters a and b unknown to him. Bob's task is to securely transfer to Alice the DV state of a single-rail qubit of the form $|\psi_{DV}\rangle_4 = (a\,|0\rangle + b\,|1\rangle)_4$. The actions of the four parties in this case are shown in Figure 8b. We also calculate the average probability of success and the average fidelity.

CHAPTER 3. HYPERENTANGLEMENT AND ITS APPLICATIONS FOR CONTROLLED BIDIRECTIONAL REMOTE HYPERSTATE PREPARATION AND CONTROLLED REMOTE IMPLEMENTATION OF OPERATORS

In this chapter, we examine in detail the following two problems related to hyperentanglement. In Section 3.1 we proposed the bidirectional remote hyperstate preparation scheme under common quantum control using hyperentanglement. In Section 3.2 we research the scheme of controlled remote implementation of operators via hyperentanglement.

3.1. Bidirectional remote hyperstate preparation under common quantum control using hyperentanglement

3.1.1. The working quantum channel

The task of our concern involves three parties who are far apart from each other: Alice and Bob being the two hyperstate preparers and Charlie the supervisor. Suppose that Alice has a photon whose state $|\psi\rangle$ is encoded in both P-DOF and S-DOF, *i.e.*,

$$|\psi\rangle = \alpha_{00}\,|Ha_0\rangle + \alpha_{01}\,|Ha_1\rangle + \alpha_{10}\,|Va_0\rangle + \alpha_{11}\,|Va_1\rangle\,. \tag{37}$$

While Bob's photon state $|\phi\rangle$ has the form

$$|\phi\rangle = \beta_{00}\,|Hb_0\rangle + \beta_{01}\,|Hb_1\rangle + \beta_{10}\,|Vb_0\rangle + \beta_{11}\,|Vb_1\rangle\,. \tag{38}$$

We find out that the above-said task could be achieved if the three participants are beforehand connected by a quantum channel whose state reads

$$|\Gamma\rangle_{12345} = \left|\Gamma^{(S)}\right\rangle_{12345}\left|\Gamma^{(P)}\right\rangle_{12345}, \tag{39}$$

with

$$\begin{aligned}\left|\Gamma^{(S)}\right\rangle_{12345} &= \frac{1}{2}[|a_0b_0\rangle\,(|c_0d_0e_0\rangle + |c_1d_1e_1\rangle)\\ &\quad + |a_1b_1\rangle\,(|c_0d_0e_1\rangle + |c_1d_1e_0\rangle)]_{12345}\end{aligned} \tag{40}$$

and

$$\begin{aligned}\left|\Gamma^{(P)}\right\rangle_{12345} &= \frac{1}{2}[|HH\rangle\,(|HHH\rangle + |VVV\rangle)\\ &\quad + |VV\rangle\,(|HHV\rangle + |VVH\rangle)]_{12345}.\end{aligned} \tag{41}$$

The production of $|\Gamma\rangle_{12345}$ starts from the following initial state

$$|\Phi_0\rangle_{12345} = \left|\Phi_0^{(S)}\right\rangle_{12345}\left|\Phi_0^{(P)}\right\rangle_{12345}, \tag{42}$$

where

$$\left|\Phi_0^{(S)}\right\rangle_{12345} = |a_0b_0c_0d_0e_0\rangle_{12345} \tag{43}$$

and

$$\left|\Phi_0^{(P)}\right\rangle_{12345} = |HHHHH\rangle_{12345} \tag{44}$$

which can be treated separately because manipulating the S-DOF cause no effects on the P-DOF and vice versa. Let us first deal with $\left|\Phi_0^{(S)}\right\rangle_{12345}$ which are sketched in Figure 9. Next, we move on to the process of generating the entangled state at P-DOF, $\left|\Gamma^{(P)}\right\rangle_{12345}$, which is depicted in Figure 10.

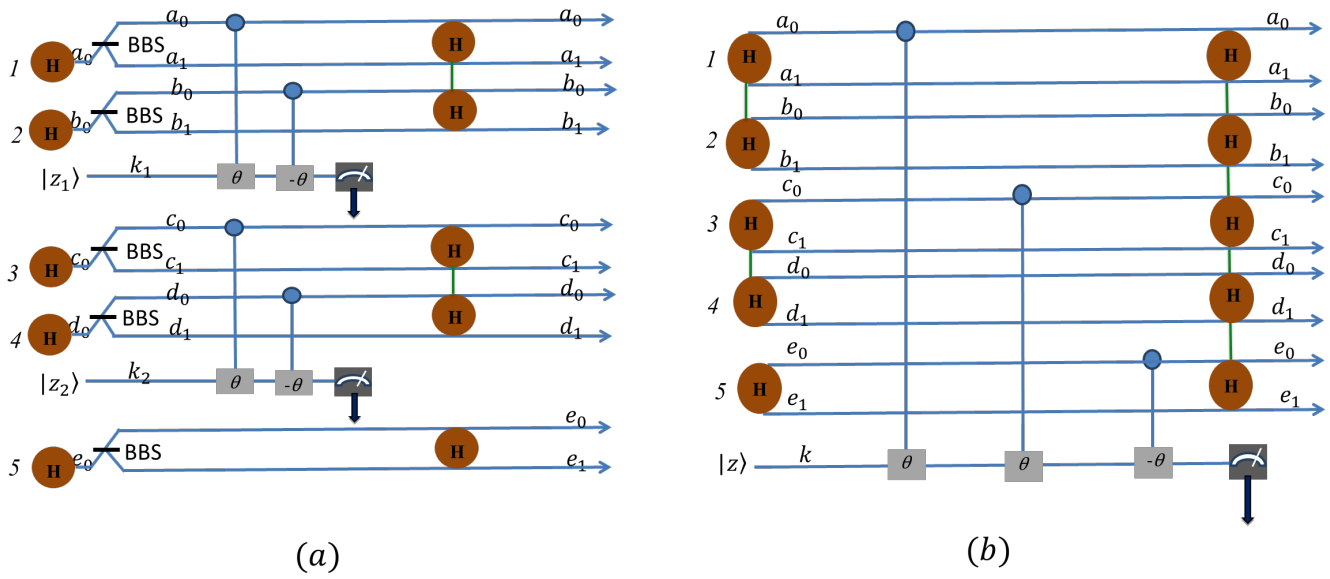

Figure 9: Scheme for production of the state $|\Gamma^{(S)}\rangle_{12345}$ in (40).

3.1.2. Controlled bidirectional remote hyperstate preparation

Once the five-photon hyperentangled state (39) has been produced it can be employed as a working quantum channel to perform the controlled bidirectional remote hyperstate preparation protocol mentioned previously. The hyperentangled state $|\Gamma\rangle_{12345}$ should be shared in such a way that Alice holds photons 1 and 3, Bob holds photons 2 and 4 while Charlie holds photon 5. In order to achieve unit success probability Alice, Bob and Charlie should agree in proper co-operations as will be detailed below (see Figure 11).

3.2. Controlled remote implementation of operators via hyperentanglement

3.2.1. Controlled remote implementation of operators (CRIO) on photon state in S-DOF

Let Alice and Bob be two partners who are under control of Charlie. The three people are in remote places and can communicate via classical means only. Alice has a photon a with certain polarization which propagates simultaneously along two distinct spatial paths x_0 and x_1. Without loss of generality we assume that

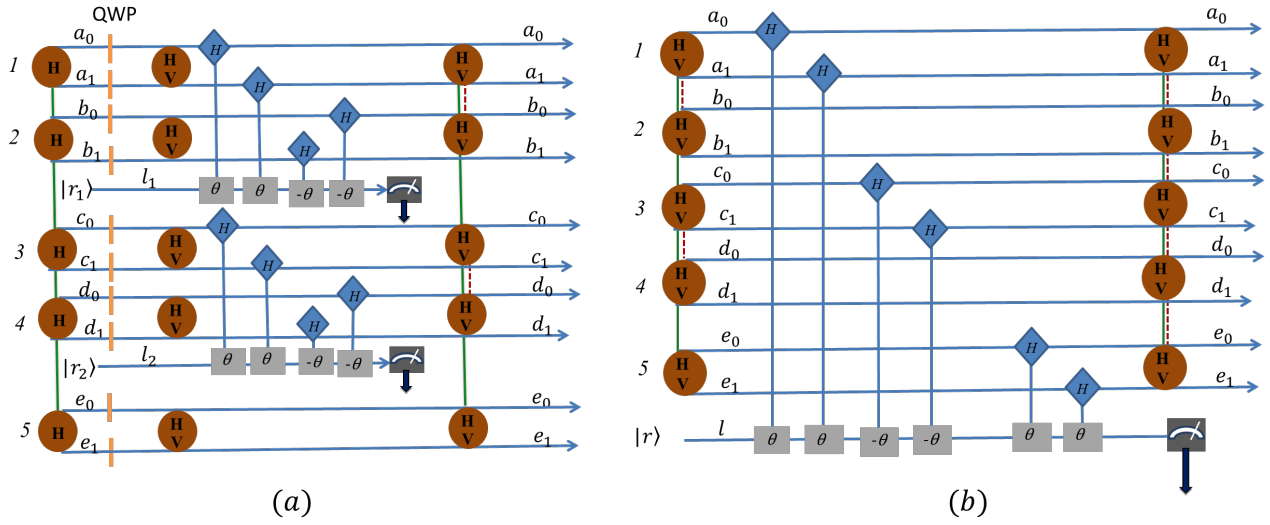

Figure 10: Scheme for production of the state $|\Gamma^{(P)}\rangle_{12345}$ in (41).

the photon polarization is vertical (V), thus Alice's photon state is of the form

$$|\psi\rangle_a = \left|\psi^{(S)}\right\rangle_a |V\rangle_a , \tag{45}$$

$$\left|\psi^{(S)}\right\rangle_a = (\alpha\,|x_0\rangle + \beta\,|x_1\rangle)_a. \tag{46}$$

Bob is equipped with an apparatus that executes a general unitary operator

$$U^{(S)} = \begin{pmatrix} u & v \\ -v^* & u^* \end{pmatrix} \tag{47}$$

on any single-photon state in S-DOF. The first task is to design a protocol for Alice and Bob to cooperate under Charlie's control so that at the end, upon approval of Charlie, Alice will hold a photon in the state

$$U^{(S)}\,|\psi\rangle = (U^{(S)}\left|\psi^{(S)}\right\rangle)\,|V\rangle = \left|\psi'^{(S)}\right\rangle |V\rangle\,. \tag{48}$$

For the first task of CRIO mentioned above, we employ one three-photon hyper-entangled GHZ state

$$\left|Q^{(SP)}\right\rangle_{ABC} = \left|Q^{(S)}\right\rangle_{ABC} \left|Q^{(P)}\right\rangle_{ABC}, \tag{49}$$

$$\left|Q^{(S)}\right\rangle_{ABC} = |a_0\rangle_A\,|b_0\rangle_B\,|c_0\rangle_C + |a_1\rangle_A\,|b_1\rangle_B\,|c_1\rangle_C\,, \tag{50}$$

$$\left|Q^{(P)}\right\rangle_{ABC} = |H\rangle_A\,|H\rangle_B\,|H\rangle_C + |V\rangle_A\,|V\rangle_B\,|V\rangle_C\,. \tag{51}$$

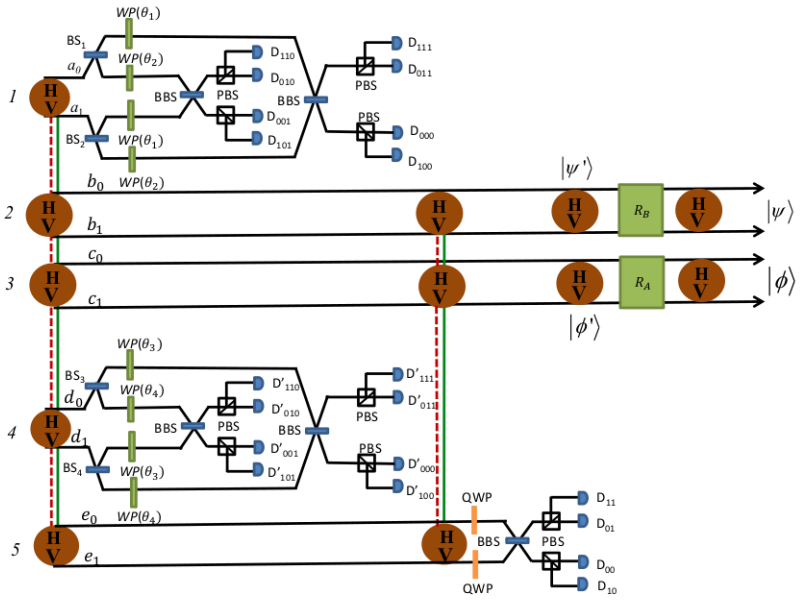

Figure 11: Scheme for controlled bidirectional remote hyperstate preparation.

The CRIO task consists of two steps. In the first step only the S-DOF part of the quantum channel (*i.e.*, $\left|\Phi^{(S)}\right\rangle_{aABC}$) is exploited. This step is shown in Figure 12. In the second step, we consider the P-DOF component of the quantum channel, $\left|\Phi^{(P)}\right\rangle_{aABC}$. This step is shown in Figure 13.

3.2.2. CRIO on photon state in P-DOF

In this section we are concerned with Alice having a photon a which has the form

$$|\phi\rangle_a = \left|\psi^{(P)}\right\rangle_a |x\rangle_a , \tag{52}$$

$$\left|\psi^{(P)}\right\rangle_a = (\gamma\,|H\rangle + \delta\,|V\rangle)_a, \tag{53}$$

with $|\gamma|^2 + |\delta|^2 = 1$. The apparatus of Bob is now capable of executing a general unitary operator

$$U^{(P)} = \begin{pmatrix} \zeta & \eta \\ -\eta^* & \zeta^* \end{pmatrix} \tag{54}$$

on $\left|\psi^{(P)}\right\rangle$ as

$$U^{(P)} \left|\psi^{(P)}\right\rangle = \gamma'\,|H\rangle + \delta'\,|V\rangle = \left|\psi'^{(P)}\right\rangle, \tag{55}$$

$$\gamma' = \gamma\zeta - \delta\eta^*, \delta' = \gamma\eta + \delta\zeta^*. \tag{56}$$

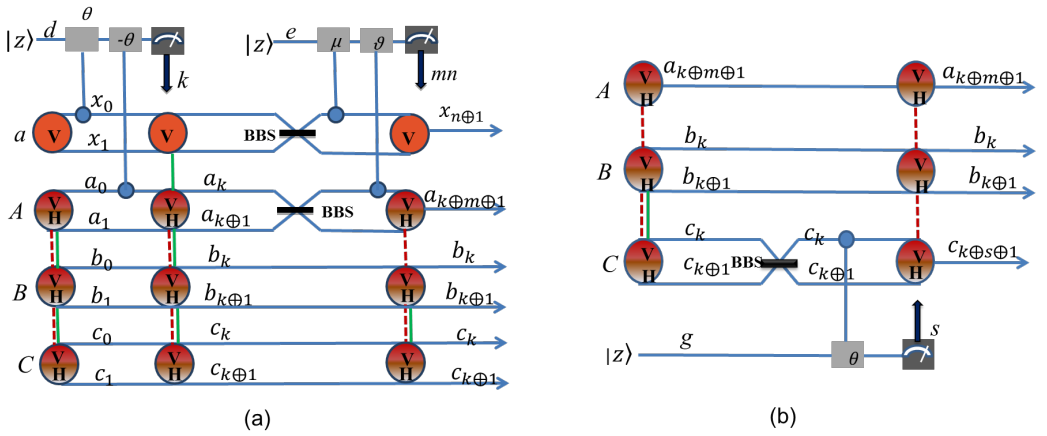

Figure 12: The first step of CRIO on photon state in S-DOF

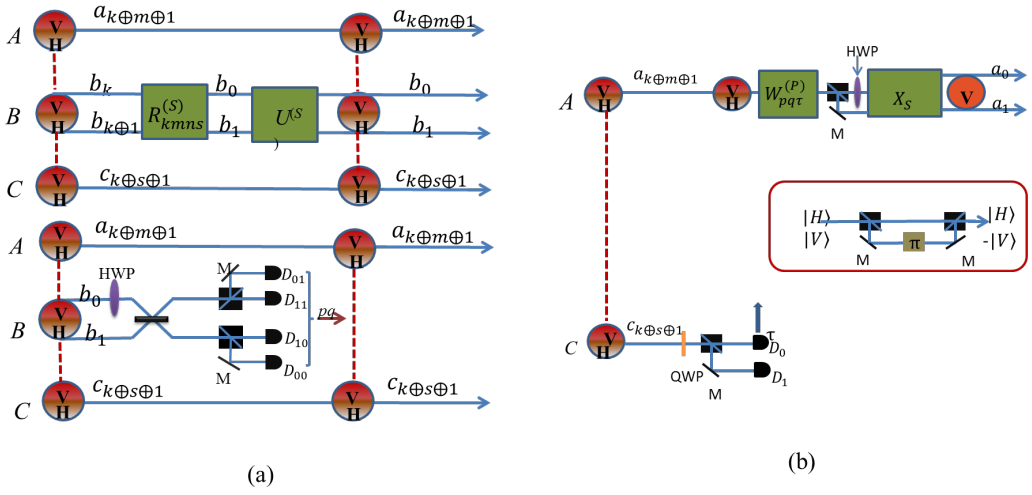

Figure 13: The second step of CRIO on photon state in S-DOF.

The second task of our concern is to design a protocol for CRIO on P-DOF state: Alice and Bob, under Charlie's control, should cooperate in order that upon completion of the protocol Alice will have at hand the state

$$U^{(P)}\left|\phi\right\rangle = \left|\psi'^{(P)}\right\rangle\left|x\right\rangle . \tag{57}$$

This task can also be fulfilled in two steps using the same hyperentangled GHZ state (49). The first step is manipulated only with P-DOF $\left|\Phi^{(P)}\right\rangle_{aABC}$ and is shown in Figure 14. Step 2 is manipulated with the S-DOF component and is shown in Figure 15.

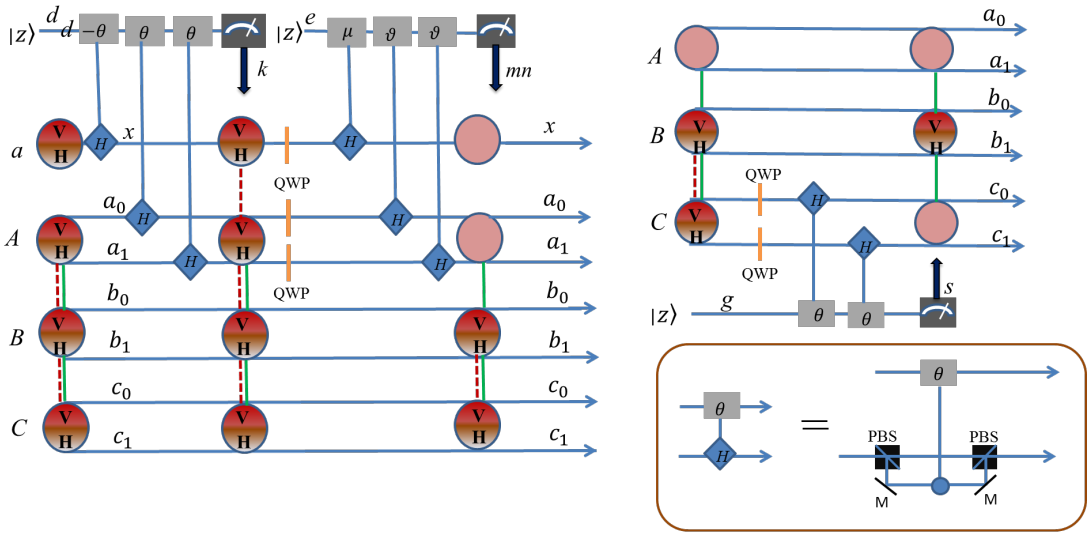

(a) (b)

Figure 14: The first step of CRIO on photon state in P-DOF.

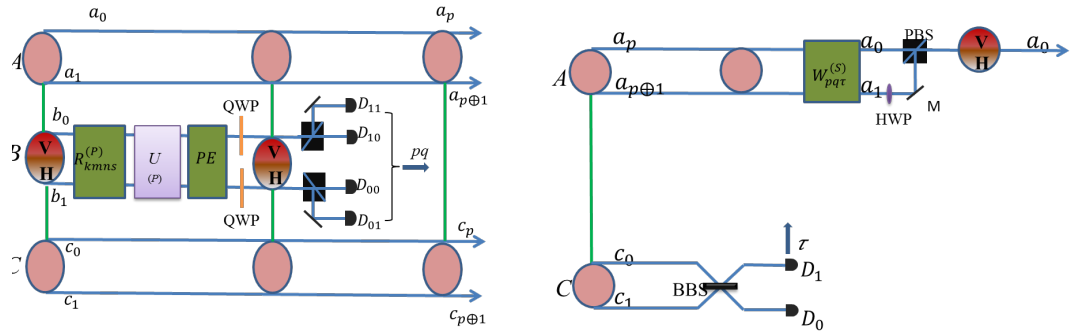

(a) (b)

Figure 15: The second step of CRIO on photon state in P-DOF.

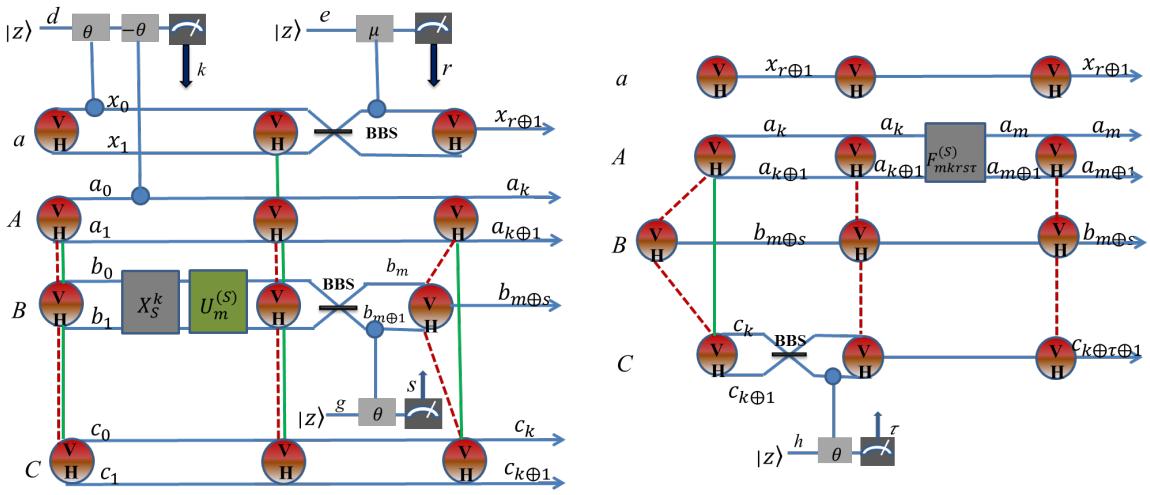

Figure 16: The first step of CRISO on photon state in both S-DOF and P-DOF.

3.2.3. CRISO on photon state in both S-DOF and P-DOF

This section gives a third task which is controlled remote implementation of a subset of operators (CRISO) on photon state encoded at the same time in both S-DOF and P-DOF. We shall propose a protocol for CRISO in which the operators belong to the following subset of unitary operators $U_m^{(S)} \in \{U_0^{(S)}, U_1^{(S)}\}$ and $U_n^{(P)} \in \{U_0^{(P)}, U_1^{(P)}\}$ with

$$U_0^{(S)} = \begin{pmatrix} s_0 & 0 \\ 0 & s_0^* \end{pmatrix}, \; U_1^{(S)} = \begin{pmatrix} 0 & s_1 \\ -s_1^* & 0 \end{pmatrix}, \tag{58}$$

$$U_0^{(P)} = \begin{pmatrix} p_0 & 0 \\ 0 & p_0^* \end{pmatrix}, \; U_1^{(P)} = \begin{pmatrix} 0 & p_1 \\ -p_1^* & 0 \end{pmatrix}. \tag{59}$$

The CRISO protocol also consists of two step. The first step only considers the S-DOF component $\left|\Phi^{(S)}\right\rangle_{aABC}$ and is shown in Figure 16. The second step operates on the P-DOF component and is shown in Figure 17.

CONCLUSION

In this thesis, we study two types of entanglement, hybrid entanglement and hyperentanglement. We also consider their applications in quantum information

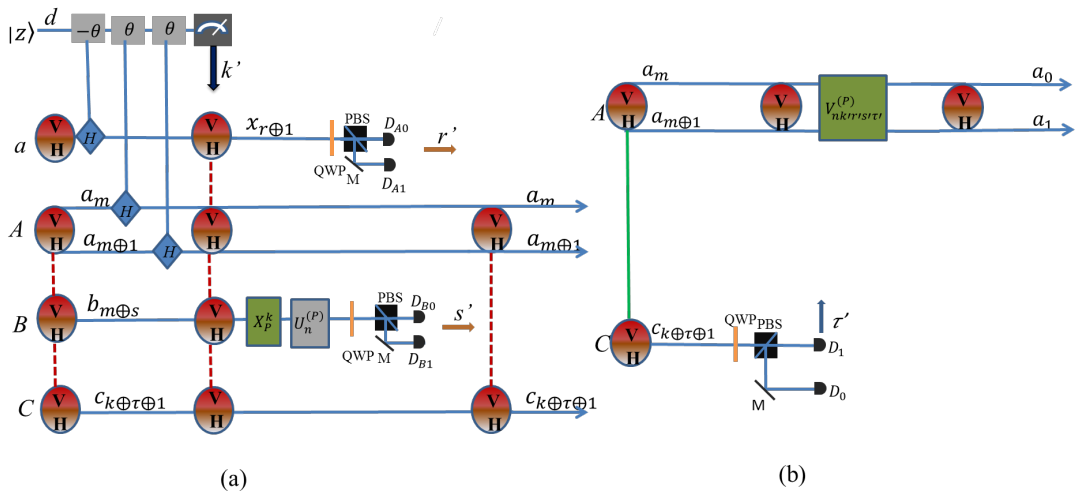

Figure 17: The second step of CRISO on photon state in both S-DOF and P-DOF.

processing.

Firstly: We have successfully built a two-mode hybrid entangled state between the polarized coherent state and the single-photon polarization state of the form as shown in the formula (3).

Secondly: We have first suggested a scheme to prepare an appropriate hybrid four-party pure entangled state which after the sharing process among the four authorized parties through a lossy environment is dissipated and becomes a mixed one. We then use this mixed state as the working quantum channel to perform controlled teleportations between a single-rail and a coherent-state qubits.

Thirdly: We have designed an optical scheme to produce a five-photon ten-qubit hyperentangled state which can be used as the shared quantum channel for Alice and Bob to prepare for each other a single-photon two-qubit hyperstate under common control of Charlie.

Fourthly: We have put forward three tasks of deterministic controlled implementation of operators on remote photon states. The first task deals with general operators and photon states in S-DOF. For the second task the operator is also general but the photon state is in P-DOF. The third task however concerns particular subsets of operators with photon states being in both S-DOF and P-DOF.

LIST OF PUBLICTIONS USED FOR THESIS

1. Dat Thanh Le, Cao Thi Bich, Nguyen Ba An, "Feasible and economical scheme to entangle a polarized coherent state and a polarized photon", Optik - International Journal for Light and Electron Optics **225**, 165820 (2021).
2. Cao Thi Bich and Nguyen Ba An, "Teleporting DV qubit to CV qubit and vice versa via DV-CV hybrid entanglement across lossy environment supervised simultaneously by both DV and CV controllers", Pramana – J. Phys. **96**, 33 (2022).
3. Nguyen Ba An and Bich Thi Cao , "Controlled remote implementation of operators via hyperentanglemen", J. Phys. A: Math. Theor. **55,** 225307 (2022).
4. Cao Thi Bich and Nguyen Ba An, "Bidirectional remote hyperstate preparation under common quantum control using hyperentanglement", Journal of the Optical Society of America B **1,** 11 (2023).